Journal of Molecular Spectroscopy 348 (2018) 152–160

Contents lists available at ScienceDirect

Journal of Molecular Spectroscopy

journal homepage: www.elsevier.com/locate/jms

Comparative SIFT-MS, GC–MS and FTIR analysis of methane fuel produced in biogas stations and in artificial photosynthesis over acidic anatase TiO_2 and montmorillonite

Antonín Knížek [a,b], Ksenyia Dryahina [a], Patrik Španěl [a], Petr Kubelík [a,c], Ladislav Kavan [a], Markéta Zukalová [a], Martin Ferus [a,*], Svatopluk Civiš [a,*]

[a] J. Heyrovský Institute of Physical Chemistry, Czech Academy of Sciences, Dolejškova 3, CZ 18223 Prague 8, Czech Republic
[b] Charles University in Prague, Faculty of Science, Department of Physical and Macromolecular Chemistry, Albertov 2030, CZ12840 Prague 2, Czech Republic
[c] Department of Radiation and Chemical Physics, Institute of Physics, Czech Academy of Sciences, Na Slovance 1999/2, CZ18221 Prague 8, Czech Republic

ARTICLE INFO

Article history:
Received 29 August 2017
In revised form 3 October 2017
Accepted 4 October 2017
Available online 5 October 2017

Keywords:
SIFT-MS
FTIR
Biogas analysis
Photocatalytic reduction
Global warming
Carbon dioxide

ABSTRACT

The era of fossil fuels is slowly nearing its inevitable end and the urgency of alternative energy sources basic research, exploration and testing becomes ever more important. Storage and alternative production of energy from fuels, such as methane, represents one of the many alternative approaches. Natural gas containing methane represents a powerful source of energy producing large volume of greenhouse gases. However, methane can be also produced in closed, CO_2-neutral cycles. In our study, we compare detailed chemical composition of CH_4 fuel produced in two different processes: Classical production of biogas in a rendering station, industrial wastewater treatment station and landfill gas station together with novel approach of artificial photosynthesis from CO_2 over acidic anatase TiO_2 in experimental apparatus developed in our laboratory. The analysis of CH_4 fuel produced in these processes is important. Trace gaseous traces can be for example corrosive or toxic, low quality of the mixture suppresses effectivity of energy production, etc. In this analysis, we present a combination of two methods: High resolution Fourier transform infrared spectroscopy (HR-FTIR) suitable for the main component analysis; and the complementary extremely sensitive method of Selected Ion Flow Tube Mass Spectrometry (SIFT-MS) and gas chromatography (GC–MS), which are in turn best suited for trace analysis. The combination of these methods provides more information than any single of them would be able to and promises a new possible analytical approach to fuel and gaseous mixture analysis.

1. Introduction

Renewable sources of energy are becoming more and more important in the modern era of energy management on Earth and many studies have been published in this field during the last few decades. The aim of most of these studies was to discover a way to harvest solar power. This could ideally save the ever more endangered environment by reducing the need for fossil fuels and so minimizing the destruction of land by mining and also lowering the rising levels of carbon dioxide in the atmosphere [1]. The levels of carbon dioxide in 2012 have averaged 395 ppm [1] and are found to be 407.25 ppm in 2017 (July, Mauna Loa Observatory [2]), while in the preindustrial era, the levels averaged 270 ppm [3]. Humankind produced about 30.4 Gt of carbon dioxide per year into the atmosphere and the number is still increasing with estimated of about 40 Gt released per year [4]. The part humankind has played in this increase of carbon dioxide levels is non-debatable. Higher levels of carbon dioxide in the atmosphere boost the greenhouse effect which in turn warms our home planet. Not only does CO_2 act as a greenhouse gas itself but the higher temperature it generates also means that more water is evaporated into the atmosphere. Water vapour is much more efficient as a greenhouse gas and therefore the global warming is accelerated. Also, as the partial pressure of carbon dioxide is rising in the atmosphere, more of the gas is dissolved into the ocean than ever. CO_2 reacts with water to form HCO_3^-. The pH of the ocean is therefore being lowered which has significant negative effects on the fauna and the flora. Also, exploitation of rainforests significantly depressed CO_2 absorption capacity in nature. The natural carbon dioxide cycle involves currently about 90 Gt of CO_2 [3] which the

* Corresponding authors.
E-mail addresses: martin.ferus@jh-inst.cas.cz (M. Ferus), svatopluk.civis@jh-inst.cas.cz (S. Civiš).

https://doi.org/10.1016/j.jms.2017.10.002
0022-2852/

flora, microorganisms and underground inorganic materials are currently able to uptake. Lowering the amount of flora in the rainforests by logging and in oceans by lowering the pH means that the natural capacity to mitigate our environmental-unfriendly actions is almost negated.

Classical biogas [5] is a versatile renewable energy source which consists of a mixture of methane and carbon dioxide together with nitrogen, oxygen and trace amounts of various substances (Volatile Organic Compounds – VOCs, sulphur compounds) which emerge mainly from the reaction space for waste degradation [6]. Biogas is currently most widely used as a fuel for generating electricity or heat, usually only on a local scale. The solid leftover from this process may be used as a fertilizer. The composition of biogas is usually determined by gas chromatography (GC) as the main separation method. These analyses often use thermal conductivity (TCD), flame ionization (FID) or mass spectrometry (MS) detectors. Other techniques include the use of infrared spectroscopy and electroanalytical methods.

Artificial photosynthesis represents different kind of a process. The chain of reactions is characterized by a homogeneous mechanism catalysed by metal complexes which act as both light antennas and catalysts [7]. In terms of carbon-cycle, biogas production is based on decomposition of a biomass, in which CO_2 is fixed. This gas is released together with energy in decomposition of methane, so the process involving biotic photosynthesis and biotic anaerobic production of methane is CO_2-neutral. Artificial photosynthesis directly involves abiotic consumption of CO_2 and production of CH_4. In this manner, the fuel production is CO_2-neutral as well. In the end of the 70′s, titania catalysts were first used in aqueous suspension for photoelectrocatalytic CO_2 reduction to CH_3OH and HCHO while CO and CH_4 were detected in the gas phase [8]. In the 90′s, manifold experiments have been conducted in order to enhance this methane production, e.g. deposition of a metal on TiO_2 [9], crystal phases [10], and from the beginning of the 21 st century these explorations continued with application of aqueous suspensions [11], special reactors containing porous TiO_2 pellets [11], sophisticated nitrogen-doped titania nanotube arrays [12], systems of CuO-$TiO_{2-x}N_x$ hollow nanocubes [13], graphene oxide-TiO_2 nanocomposite [14], etc.

Several modern approaches also involve ruthenium or rhenium [15,16]. However, clear disadvantage lies in the rarity of their natural occurrence and so the costs of their production. The current state of the art is covered in its great broadness e.g. in [7,17,18] and references therein.

Both processes can be classified as CO_2-neutral renewable energy providers. Although the use of renewable energy is quickly rising, the share of renewables in the overall world energy consumption is not growing as quickly. Nevertheless, renewable energy provided an estimated 24% of global energy consumption in 2015 [19]. This represents a significant increase in comparison with the situation in 2011, when 81% of the energy needs were met by fossil fuels, while renewable sources accounted only for 13%. It should be noted that up to 20 TW can by extracted from wind, tides, biomass, and geothermal sources annually [20]. However, in 2015, the annual global energy power consumption reached up to 17.4 TW and is estimated to rise to 25–27 TW by 2050 [7]. The solar light energy reaching the Earth represents powerful source to overcome this lack of renewable sources of power in the future. In order to optimize the processes of CO_2-neutral energy production, alongside with a deep understanding of methane fuel production chemical mechanisms, the need of trace chemical analysis is of utmost importance. For instance, methane biogas produced by Industrial wastewater treatment station in Troja (Prague, Czech Republic) contains traces of unspecified silanes [21]. These compounds are decomposed by heat and so speed up excessive gas engine wear by creating silica dust. This impurity therefore excludes the utilization of this gas for standard energy production. This particular example shows the importance of trace gas analysis of biogas. Also, artificial photosynthesis is based on a contact of CO_2 with solid photocatalyst and the process can also lead to formation of side products during the CO_2 reduction.

In this paper, a new highly sensitive method of selected ion flow tube mass spectrometry (SIFT-MS) is implemented for the trace gas analysis of biogas and methane fuel produced over acidic anatase (pure or composite with graphene), a perspective photocatalytic material synthesized in our laboratory, and a common catalytically active clay montmorillonite. The method was combined with Fourier transform high-resolution infrared spectroscopy (FTIR) used for the identification of major constituents of the sample.

2. Methods

2.1. Laboratory sample preparation

2.1.1. Photocatalytic reduction of CO_2

The photocatalytic properties of three catalysts were studied: anatase, which was annealed at 200 °C (CAS 1317-70−0, TiO_2, synthesized in our laboratory as type A200 [22–28], either in composite with graphene or pure, and montmorillonite (CAS 1318-93−0, type K10, Sigma Aldrich). The A200-graphene composite was prepared by sonication of A200 in 2% aqueous suspension of graphene oxide.. The product was centrifuged, dried at 50 °C in air and then reduced at 400 °C in vacuum overnight to convert graphene oxide to graphene. The resulting A200-graphene composite was stored in a glove box in Ar atmosphere. The A200 sample contained 14 wt% of HCl as determined by titration analysis. Prior to both experiments, samples were degassed and dried in vacuum (10^{-3} Torr) at room temperature.

For each experiment, a 30 cm long (diameter 2.5 cm) glass optical cell equipped with CaF_2 windows was used. The cell was filled with 0.5 g of the following catalysts:

a) TiO_2 sample A200 (contains adsorbed HCl from the synthesis)
b) Montmorillonite dried in vacuum and saturated with 36% (w/v) HCl vapour (Sigma Aldrich, USA) until the partial pressure in the sample cell was 8 Torr (approximately 7.98 Torr for HCl and 0.02 Torr of H_2O).
c) TiO_2 sample A200 composite with graphene

Then the cell was filled with a carrier gas consisting of 10 Torr of CO_2 (Linde Gas, Germany) and 2 Torr of N_2 (Linde Gas, Germany). Both cells were irradiated with a 364 nm UV lamp with an intensity of 3000 mW cm^{-2}. The mechanism and the reprocessing of the resulting mixture main constituents are described in our previous paper [28]. The resulting mixture after the irradiation was analysed by FTIR and SIFT-MS in order to determine its composition and the content of trace amounts of compounds as is described below.

2.1.2. Biogas sample collection

Along with the analysis of the photocatalytic reduction products, samples of biogas were analysed as well. The samples were collected at standard sites of the technological process into evacuated 5 l glass cells. The cells were then transported to the laboratory and analysed by FTIR and SIFT-MS. The samples originated from biogas production facilities in Trhový Štěpánov, Czech Republic and Velký Karlov, Czech Republic, the Central wastewater treatment plant in Prague, Czech Republic and two landfills of

municipal waste in the districts Praha - Ďáblice and Praha - Dolní Chabry, Prague, Czech Republic.

2.2. FTIR analysis

The spectra of the biogas samples were measured using the Bruker IFS 120 (Bruker Optics, Germany) spectrometer in the spectral range 650–5500 cm^{-1}. In order to cover the near-infrared (NIR) range a halogen lamp, a CaF_2 beam splitter and InSb detector were used, and to cover the middle-IR (MIR) spectral region a glow bar source, KBr beam splitter and HgCdTe detector were applied. Fifty scans of the spectra were acquired at the resolution of 0.02 cm^{-1} using the Blackmann–Harris apodization function.

The spectra were measured using the Bruker IFS 125 HR spectrometer (Bruker Optics, Germany) equipped with a KBr beam splitter and a nitrogen cooled InSb detector over the spectral range of 1800–6000 cm^{-1} in regular intervals. Spectra were measured with a resolution of 0.02 cm^{-1} using the Blackmann-Harris apodization function [29].

Concentrations of CO_2, CO and CH_4 were determined by independent calibration using pure gases (CO_2, CO, and CH_4) diluted with nitrogen buffer gas. The integrated intensities of the selected individual absorption lines were calculated using the OPUS 6.0 software package [30], and the data were subsequently manually fitted by a linear regression model.

2.3. SIFT-MS analysis

The selected ion flow tube mass spectrometry (SIFT-MS) method is based on soft chemical ionization by selected reagent ions of a gaseous sample introduced into a flow tube (see [31]). Reagent ions were created in a gas discharge ion source, selected by a quadrupole mass filter and injected into a stream of fast flowing helium carrier gas. Sample gas was introduced into the carrier gas/reagent ion swarm via a calibrated capillary at a known flow rate (see Fig. 1). The capillary and the connecting tubes were heated to approximately 100 °C to inhibit the condensation of water vapour and other compounds from the sample onto the tube surfaces. The reagent ions used for SIFT-MS analyses were H_3O^+, NO^+ and O_2^+. These ion species do not react with the major components of air (N_2, O_2, H_2O, CO_2 and Ar) but usually react rapidly with most volatile organic compounds. Notable exceptions are the low molecular weight alkanes, CH_4, C_2H_6 and C_3H_8, which do not react rapidly with organic compounds; however there is a slow reaction of O_2^+ with methane that can be used for its quantification at concentrations above 1000 ppm. H_3O^+ reagent ions associate with water vapour molecules present in the sample producing the hydrated hydronium ions, $H_3O^+.(H_2O)_{1,2,3}$. Typically, H_3O^+ reactions proceed via proton transfer forming product ions at m/z = (M + 1), where M is molecular weight of the analyte molecule; however, fragments are often present especially for alcohols [32] or aldehydes [33]. The selected reagent ions, characteristic product ions and their hydrates present in the carrier gas were analysed by a downstream quadrupole mass spectrometer. Absolute concentrations of the analytes were calculated from the sample flow rate, the flow tube pressure, the known reaction time in the flow tube and the ion-molecule reaction rate coefficients. Details of this calculation are given in Ref. [34].

2.4. GC–MS analysis

GC–MS spectra were obtained on a gas chromatograph (Finnigan Focus GC, ITQ 700, Thermo Electron Corp.) with mass detection (Xcalibur ion trap, Thermo Scientific). 10 μL of each sample gas phase was injected into the column at 200 °C. Helium was used as a carrier gas with 0.3 ml min^{-1} flow. The separation lasted 14.50 min. After the separation, the sample was ionized with 70 eV electron stream and transferred to the ion trap. The spectra were assigned using Thermo Xcalibur in-built library.

3. Results and discussion

Using combination of FTIR, SIFT-MS and GC–MS techniques, we have examined chemical composition of biogas and methane fuel produced in biogas stations and by photocatalytic reactions, respectively. Our photocatalysts were based on acidic anatase and montmorillonite. In case of montmorillonite, its photocatalytic activity in production of methane was published to the best of our knowledge for the first time by our group. In the following chapters, particular results are discussed in details.

3.1. Rendering biogas analysis

The FTIR spectrum of rendering biogas from Trhový Štěpánov is shown in Fig. 1.

Apart from methane, water and CO_2, no other compounds were detected as their concentration was below the detection limit of the spectrometer (about 10–100 ppm depending on band strength). We show exclusively this spectrum as an example of typical FTIR spectrum of biogas, due to similarity in absorption bands exhibiting in this spectral record as well as in spectra of other biogases. In terms of fundamental spectroscopy, apart from strong fundamental vibrations, spectral record is characteristic with a wide range of CO_2 and CH_4 combination bands. CO_2 exhibits fundamental vibrations [35] υ_2 and υ_3 (667 and 2349 cm^{-1} respectively), strong well known combinations bands [36] $2\upsilon_2 + \upsilon_3$ and $\upsilon_1 + \upsilon_3$ (3600 and 3705 cm^{-1} respectively) and Fermi Triad sequence

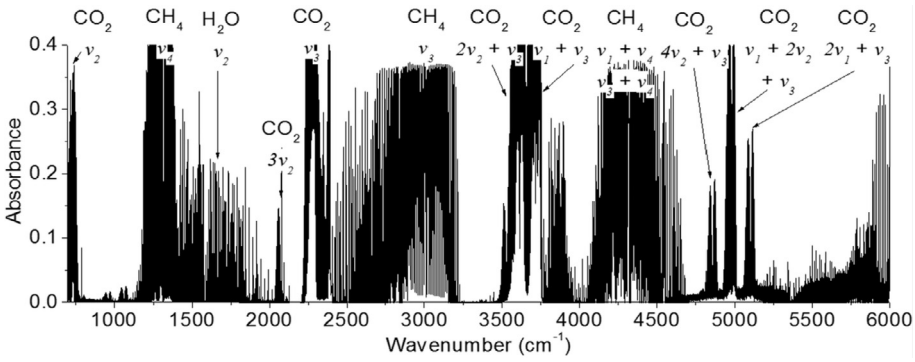

Fig. 1. Survey of Trhový Štěpánov biogas infrared spectrum.

[37] of $4\nu_2 + \nu_3$, $\nu_1 + 2\nu_2 + \nu_3$ and $2\nu_1 + \nu_3$ (4853 cm^{-1}, 4978 and 5099 cm^{-1}). Spectrum of methane exhibits strong fundamental [35] ν_4 and ν_3 bands (1306 and 3019 cm^{-1}) together with a series of combination bands [38,39] $\nu_1 + \nu_4$, $\nu_3 + \nu_4$ and $\nu_2 + \nu_3$ (4220, 4320 and 4540 cm^{-1}). It should be noted that such strong combination bands in the near infrared region intend biogas as ideal subject for further exploration of simple gas sensors based for instance on novel wafer-fused vertical-cavity surface-emitting lasers in combination with a cheap InGaAs photodiode that can operate at room temperature in the 1.2–2.6 μm wavelength range [40]. However, in our study, methane, water and carbon dioxide concentrations were quantified using calibration gases.

Composition of rendering biogas has been also examined using mass spectrometry. The SIFT-MS method is suitable for determining the concentration of traces and struggles with analyses of components with cations of % concentration in the sample. Some species are also difficult to detect with this technique, e.g. N_2, O_2, CO_2, CO, H_2 and small aliphatic hydrocarbons (up to C_4). Mutual interference of some compounds may also be problematic. For example the quantification of acetylene is troublesome, because of the reactions (1) & (2):

$$CH_4 + C_2H_2^+ = C_3H_5^+ + H\cdot \quad (1)$$

$$CH_4 + C_2H_2^+ = CH_3CCH^+ + H_2 \quad (2)$$

These reactions in effect lower the amount of CH_4 and $C_2H_2^+$ in the sample and distort the quantification. Also, even though CH_4 reacts with H_3O^+ (3),

$$CH_4 + H_3O^+ = CH_3O_2 + H\cdot \quad (3)$$

the reaction is very slow ($k = 5.2 \times 10^{-12}$ cm^3 s^{-1}) [41]. The speed of the reaction prevents efficient determination during the continuous analysis. From this point of view, FTIR is much more suitable for determining CH_4 content.

To summarize the results of FTIR and mass spectrometry, both samples from Trhový Štěpánov and Velký Karlov rendering stations contained methane and carbon dioxide in ratio 1: 1, about 8% of water and according SIFT-MS trace analysis, among others, significant concentrations of gases suitable (except of methane and other substances mentioned above) hydrogen sulphide together with carboxylic acids, ethers, alcohols, etc. A detailed survey of chemical compositions is shown in Table 1.

3.2. Wastewater plant and municipal waste landfill biogas analyses

The wastewater plant and municipal waste landfill samples of biogas were first analysed using FTIR. In fact, regarding the content of the main biogas components (CH_4 and CO_2), the infrared spectra are very similar to previous records of rendering biogas stations. Therefore, we do not depict these spectra again. The results are shown in Table 1. In the wastewater plant sample (column Water), the amount of methane was determined to be 50%. Further, it was 48% in the Ďáblice landfill sample (column Landf. D) and 46% in the Dolní Chabry landfill sample (column Landf. C). These results show that on both landfills, there occurs a stable methanogenesis phase. This phase is typical for 40 – 60% of methane fraction in the biogas and after the landfill is closed down, the amount of methane readily decreases. Among traces detected by SIFT-MS, the most prominent was H_2S, especially in the Ďáblice landfill sample (column Landf. D). Overall, this sample contained higher amount of trace gases such as alcohols, acids, acetone, ammonia, hydrocarbons etc., which is in agreement with the fact, that the site is relatively new and still in use.

In this case, we should note the problematic quantification of H_2S, because it has proton affinity close to that of water (PA(H_2S) = 700 kJ mol^{-1}, PA(H_2O) = 691 kJ mol^{-1}. Despite its similarity, it was found that a reaction between those two occurs during the analysis (4):

$$H_3O^+ + H_2S = H_3S^+ + H_2O \quad (4)$$

This reaction does not take place with organosulphides so these are possible to quantify. Hydrogen sulphide is released during decomposition of the acidogenic phase at acidic pH. Solid municipal waste contains relatively large amounts metals which help to degrade H_2S. Metal waste is intensively corroded during these processes and the anoxic environment stabilizes mainly Fe^{3+} ions in the liquid phase. During the methanogenesis, these ions act as the main sorbents for H_2S. The following reactions sum up the process:

$$Fe = Fe^{2+} + 2e^- \quad (5)$$

$$Fe^{2+} + H_2S = FeS + 2H^+ \quad (6)$$

Iron sulphide is the product of the main degradation pathway of H_2S. Among other important organosulfur compounds there are dimethylsulphide, ethanethiol, carbon disulphide and hydrogen sulphide.

In the case of dimethylsulphide, the product during the analysis is a protonised molecule. The protonised molecule reacts with water. The same applies for ethanethiol. For example in the sample from the landfill in Dolní Chabry, 6.858 ppm of ethanethiol was found. The sample from the wastewater plant contained 12.690 ppm and the sample from Ďáblice landfill contained 8.952 ppm. In all samples, the amount belongs to the interval 0–20 ppm. In the sample from Dolní Chabry, acetic acid, propionic acid and butyric acid were found. In the Ďáblice landfill sample, the same acids were found as well but their concentration was orders of magnitude higher. Furthermore, valeric and caproic acids were found in this sample. In the biogas from the wastewater plant, all of these acids were found but their concentrations were lower. All these acids were detected using H_3O^+ ionization on the SIFT-MS and the reaction products were either protonised acids or water adducts.

We have further detected alcohols (methanol, ethanol, propanol, butanol and pentanol in the sample from Dolní Chabry, Ďáblice and the wastewater plant). Their concentrations followed the same trend with them being highest in the sample from Ďáblice. All alcohols were detected by the reaction with H_3O^+ and their water adducts same as it was with the acids. Among other detected compounds were ethylacetate, which was detected with the same reactions.

In general in the literature, it is deemed possible to obtain 50–75% of methane in the biogas. Higher yield can be obtained using technologically more complicated multistep process. Furthermore, if the substrate contains larger amounts of proteins and hydrocarbons, the production of biogas is less efficient than in the case of lipids. The methane content is also lower when warm and hot fermentations are used, in contrast to fermentation at lower temperatures.

3.3. Analysis of methane fuel produced by artificial photosynthesis

Our previous results showed that acidic protons significantly boosted the photoreduction of CO_2 [28]. In this study, we used hydrochloric acid, because it remains as the main donor of protons in photochemically very active material of anatase synthesized by laboratory wet process [27]. In order to test photocatalytic properties of montmorillonite and graphene composite TiO_2, 30% HCl solution in water was added to the montmorillonite and graphene composite TiO_2 samples prior to the UV irradiation. Gas phase of all

Table 1
Complete results achieved for biogas Ďáblice and Dolní Chabry Prague landfill stations (columns Landf. D and Landf. C respectively), Prague Central wastewater treatment plant in Troja (column Water), rendering stations Velký Karlov and Trhový Štěpánov (Rende. 1 and 2 respectively) and methane fuel produced in artificial photosynthesis over acidic anatase (column A200), acidic anatase with graphene (column A200G) and montmorillonite (column Mont.). The units are % vol. if indicated or ppb. In cases when the compound was not analysed in the sample, the corresponding table cell was left void.

Compound	Landf. D	Landf. C	Water	Rende. 1	Rende. 2	A200	A200G	Mont.
Methane	48%	46%	50%	48%	47%	18%	0.12%	2%
Water	8%	8%	4%	4%	7%	0.20%	0.40%	0.22%
Carbon dioxide	44%	46%	46%	48%	46%	69%	97%	97%
Carbon monoxide						12.70%	0.12%	0.25%
Dichloromethane						0.01%	0.52%	45,000 ppb
Trichloromethane						0.04%	0.81%	0.10%
Tetrachloromethane						0.17%	0.42%	0.15%
Hydrogensulfide	59,040	4161	214					
Penthanol	21,550	3656	514					
Butanic acid	19,910	2968	393					
Ethylacetate	17,070	3136	114					
Diethylether	14,470	1959	1286					
Pentanic acid	13,280		1601					
Hexanic acid	13,010		1902					
Butanol	11,480	2081	1047					
Ethylfenol	11,200	3338	1001					
Propanic acid	10,940	1478	960		470			
Ethanediol	8952							
Acetone	6976	280	234	700	3100	550		32,200
Ammonia	4654	350	345	1600	25,000			
Ethanol	4000	532	5736	2600	190			
Acetic acid	3958	1557	353	140			20,100	30,100
Acetaldehyde	3756	238	424	1100	250	14,800	28,800	67,400
Methylfenol	3597							
Propanol	3456	1877	1227	1700	1945			
Carbon disulphide	2566	1673	2374					
Fenol	1597	1094	455					
Dimethylsulfide	1534	69			250			
Ethanethiol	8952	6858	12690					
Methanol	945	262	128	1600				
Indol	583		762					
Hydrogencyanide	399	232						
Formaldehyde	187	328	426	19	30			

the samples has been analysed after 1800, 1300 and 300 h of irradiation, respectively, by FTIR and all of them contained both CO_2 and CH_4 + CO, i. e. the conversion was only partial and reached a steady state after several hundreds of hours of continuous irradiation. Fig. 2 shows the resulting FTIR spectra of CH_4 + CO mixtures after the end of the irradiation process. Panel A depicts survey on gas phase formed after artificial photolysis over anatase A200. CO and CH_4 bands are clearly visible in the spectra. Panel B shows this measurement in case of montmorillonite. In this spectrum, desorption of HCl from this catalyst can be observed. Finally, Panel C depicts spectra of gas phase resulting from irradiation of anatase A200 composite with graphene. CO and CH_4 bands are detectable, however, they are very weak.

Formation of CO instead of CO_2 represents the main difference between biogas and synthetic CH_4 fuel produced by artificial photosynthesis over acidic anatase, montmorillonite and graphene-anatase composite. Further analysis was conducted by GC–MS and SIFT-MS. Sample chromatogram of the gas phase over graphene-anatase composite is shown in Fig. 3.

The most prominent trace gases detected in all the samples from artificial photosynthesis over anatase, graphene composite anatase and montmorillonite are di-, tri- and tetrachloromethane, methoxyacetaldehyde. The reaction of CH_4 with HCl, which leads to the chlorination of methane, is important because it changes the methane-CO product ratio. This ratio is used in the determination of the reaction kinetics, and therefore these side reactions disturb the correct quantification of reaction rate constants. Also, the ratio of di-, tri- and tetramethylchlorides varied in each sample. In the case of graphene-anatase composite, $CHCl_3$ was most prominent and CCl_4 was the least prominent trace, whereas in the montmorillonite and pure anatase samples, CCl_4 was most abundant with CH_2Cl_2 being the least. This shows that the nature of the catalyst influences the rate of the side reactions as well. Apart from the methylchlorides, all samples contained methoxyacetaldehyde. Whether this compound is a side reaction product, a kind of product condensate or a newly discovered reaction intermediate is yet to be determined. Its role may shed more light on the reaction mechanism of the photoreduction process. In any case, this finding shows that the combination of SIFT-MS, GC–MS and FTIR is necessary for accurate analysis of biogas and biogas-like-mixture samples. Interestingly, the A200G photocatalyst, which was the least active for CO and CH_4 production, turned out to be very efficient for the generation of chlorinated hydrocarbons (Table 1).

3.4. Mechanisms of biogas and artificial photosynthesis methane fuel production

The comparative schemes of biogas production (Panel A) and artificial photosynthesis (Panel B) are depicted in Fig. 4 and further referred in this chapter.

3.4.1. Biogas production

From the biochemical point of view, the production of methane by bacteria is well-described [44]. The simplest example is methanogenic reduction of CO_2 to methane by *archaebacteria*. First, the source of CO_2 is needed. Some bacteria are able to synthesize CO_2 for themselves; some depend on other bacteria and some use CO_2 which is produced from inorganic degradation of organic matter. The reduction itself then uses methanofurane and complex

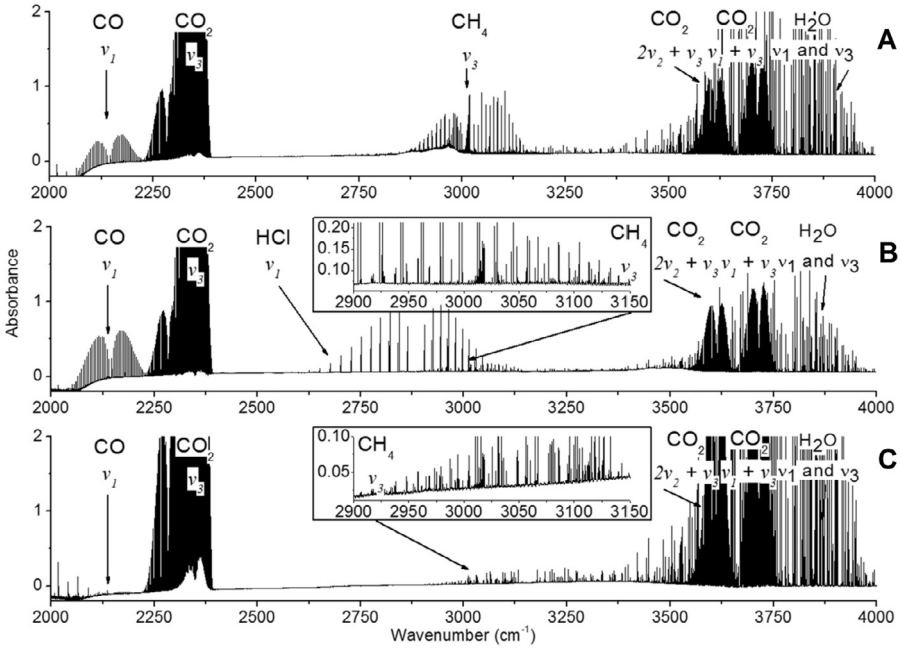

Fig. 2. FTIR survey of the gas phase methane fuel produced in artificial photosynthesis over anatase A200 (Panel A), montmorillonite (Panel B), and graphene composite with anatase A200 (Panel C).

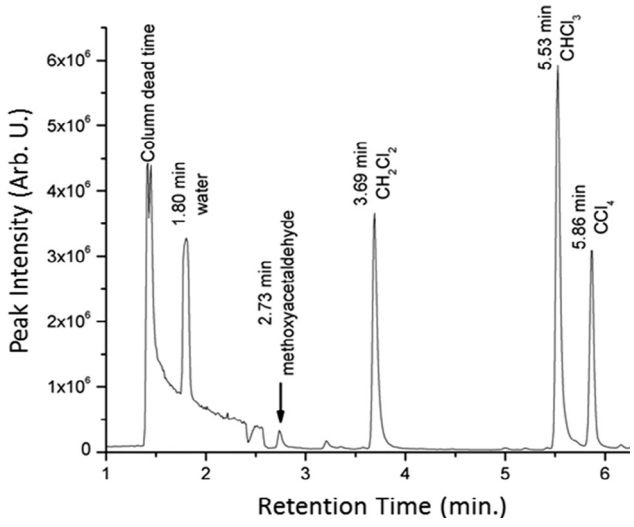

Fig. 3. Chromatographic record of gas phase produced by artificial photosynthesis over graphene-anatase composite photocatalyst in presence of HCl.

enzymatic machinery which creates an electrochemical gradient on the bacterial membrane. This proton gradient then reduces carbon dioxide step by step to methane. Another possibility is the so called 'fermentative metabolism'. This type of metabolism, which is minor in nature compared to the CO_2 based one, uses acetate as the starting compound. Acetate is decomposed to methane and carbon dioxide. The reaction is enzymatically catalysed as well. These *archaea* are referred to as *acetotrophic* or *acetoclastic*. All the methanogenic *archaea* are supposed to have evolved long before Earth's atmosphere contained oxygen. Their metabolism can therefore be regarded as an abiotic metabolism at its height. Considering and simplifying only direct degradation process of particular biomolecules, carbohydrates, lipids and proteins, the overall mechanism can be sketched based on model published by Angelidaki et al. [42]. The mechanism is depicted in Fig. 4, Panel A, "Biogas Production". Carbohydrates are converted to acetate by acidogenic bacteria and subsequently to either volatile fatty acids or methane. Lipids are degraded to glycerol and fatty acids. Glycerol is decomposed to propionate, long-chain fatty acids are degraded by acetogenic bacteria to acetate and H_2. Acetate is again decomposed to methane or carbon dioxide. Proteins are decomposed to amino acids, which are degraded mainly to acetate, propionate, butyrate, and valerate. Finally, acetate and methane together with carbon dioxide are produced.

Technologically, the anaerobic digestion consists of a series of biological and chemical processes [45] described above. In a simplified form, the process can be summarized as follows:

- Hydrolysis – This part constitutes enzymatic hydrolysis of macromolecules (polysaccharides, protein, lipids, etc.). The low molecular mass products are generally much more soluble in water than their macromolecular counterparts. This reaction is aerobic.
- Acidogenesis: During this stage, the products of the hydrolysis are transformed into acids. The environment becomes anaerobic.
- Acetogenesis: The created organic acids are transformed into the acetic acid (2-carbon compound)
- Methanogenesis: Acetotrophic bacteria utilize acetate and produce carbon dioxide and methane. Methanogenic *archaea* are then used to digest CO_2 and H_2 to produce methane, which in effect increases the yield of methane in the mixture.

In Fig. 4, Panel A, molecules detected in the samples of biogases by FTIR, GC–MS and SIFT-MS, are marked by the yellow rectangles. Among these constituents important in formation of methane and CO_2, biogas consists of other compounds (N_2, O_2, Ar, H_2, CO_2, H_2S, HCN, NH_3, hydrocarbons, their derivatives, silanes, etc.). These traces are the differentiating agents of various biogases and strongly influence the quality and usability of the biogas in industrial applications. For example, H_2S is highly corrosive and its higher concentrations shorten the lifetime of the devices used in the digestion of biomass. Silanes, which probably come from

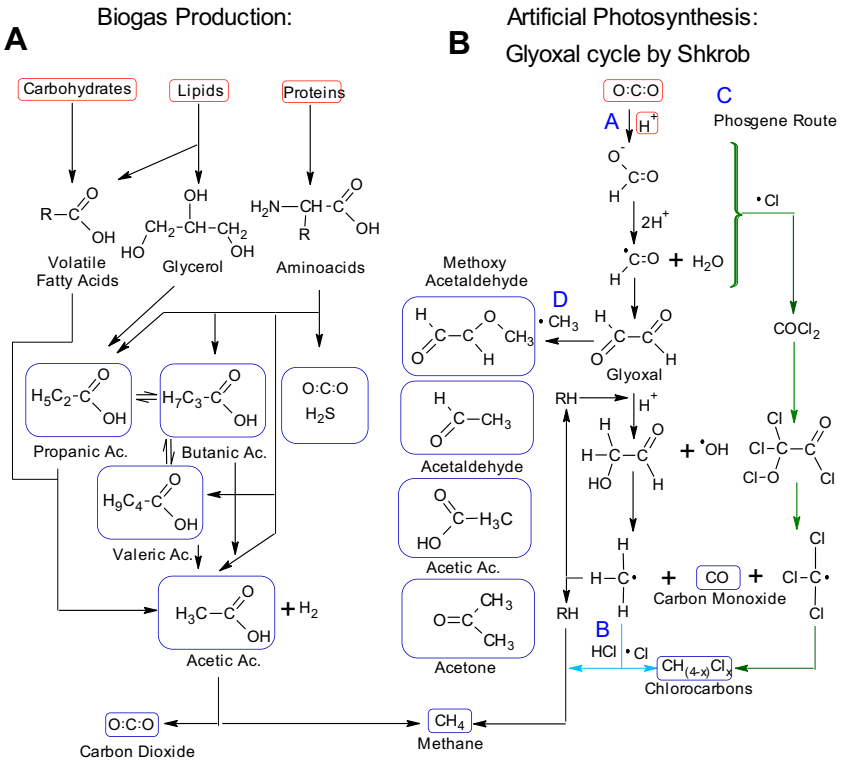

Fig. 4. Panel A shows simplified mechanisms of biogas generation comprehensively according to [42]. Panel B concludes the Glyoxal cycle [28,43] of artificial photosynthesis supplemented by results published in this study. Route B proposes our mechanism of chlorocarbons formation by direct chlorination involving $\cdot CH_3$ radical in the Glyoxal cycle. Route C concludes our new alternative mechanism of Glyoxal cycle involving formation of phosgene. Compounds in blue rectangles have been directly detected by FTIR, SIFT-MS or GC–MS in this study.

silicon oils digestion, negatively influence mechanical parts of gas-fuelled motors. From this point of view, the biogas analysis is a key to assign a correct application to a correct type of biogas.

3.4.2. Artificial photosynthesis

The photocatalytic reduction involves carbon dioxide as a source of carbon, water/acid as a source of hydrogen and a catalyst (often a metal oxide semiconductor – anatase and newly also montmorillonite in our study) serving also as a medium for electron transfer (reduction) and substrate binding of the reactants. Artificial photosynthesis produces mainly methane and carbon monoxide. In our study, we also focus on the production of trace gases. Using a combination of FTIR, GC–MS and SIFT-MS analysis, we have detected molecules shown in Table 1, column A200 for sample of anatase TiO_2 calcinated at 200 °C, A200G for this sample composite with graphene and column Mont. shows results for montmorillonite saturated with $HCl + H_2O$ vapours. After 1800 h of irradiation process the mixture still contained excess of the reactant, CO_2. However, we have observed that after about 300 h (the process is almost finished and during the next 1500 h the concentration changes negligibly. The corresponding spectra for each photocatalyst are depicted in Fig. 2.

We have estimated that the process consumes all the available acidic protons by stoichiometric calculations. The pseudo-first order fit of each dataset shows that A200 converts carbon dioxide to methane with effective rate constant of 0.006 h^{-1}, anatase A200 composite with graphene with the constant of 0.005 h^{-1} and montmorillonite with the constant of 0.0014 h^{-1}. Finally, the mixtures differ in degree of conversion: 18% of methane was quantified in case of anatase A200, 0.25% of methane in case of montmorillonite and only 0.12% of methane in case of anatase A200 composite with graphene. However, in case of montmorillonite, the real concentration of carbon monoxide was estimated to be 2%, i.e. 8× higher than calculated for methane. We assume that methane and carbon monoxide should be produced in ratio 1:1 similarly as with anatase A200. On montmorillonite, methane is probably adsorbed in this material or it is decomposed to carbon monoxide in reaction with OH radical. Nevertheless, these results point towards two unprecedented findings:

a) **Besides anatase, montmorillonite is also photochemically active.** Our previous explorations [46] of montmorillonite and several other materials show that various substances are able to adsorb CO_2 forming unstable complexes on their surface. Oxygen atoms from the crystal lattice can bind to the adsorbed molecule forming a CO_3^{2-} anion which, after internal rotation, breaks again to CO_2. This CO_2 then contains oxygen atoms from the crystal lattice. This behaviour has been experimentally demonstrated using isotope labelled CO_2 and TiO_2 together with other minerals [22–28,46–48]. Using quantum chemical calculations we have demonstrated that the oxygen exchange mechanism involves formation of a carbonate structure on TiO_2 surface near a vacancy (defect in the crystal structure). Regarding the photoreduction mechanism proposed by Shkrob [28,43] (see Fig. 4, Panel B, route A), formation of such a structure can be likely also in case of methane synthesis.

b) **Graphene composite anatase is a powerful photocatalyst to generate CH_xCl_y.** Graphene is widely used material and its composite with anatase should enhance rate of photocatalysis due to dissociation of exciton upon UV irradiation. However, our results show that composite modification does not improve the photocatalytic properties of anatase for the CO_2 reduction. While it is tempting to ascribe this effect to

shielding of UV light by the carbonaceous dark material, we must admit A200G is, on the other hand, extremely active to produce CH_xCl_y. The photocatalytic formation of CH_xCl_y over all our catalysts is shown here for the first time.

Regarding the mechanism of methane formation, our result also shows that the Glyoxal pathway depicted in Fig. 4, Panel B, route A, is very likely to come into effect for the catalysts used in this study. Overall, three plausible reaction mechanisms have been proposed so far: formaldehyde pathway [49], carbyne pathway [10] and glyoxal pathway [43]. All three of them yield various product mixtures, but all of them yield methane as the main product. All these pathways require a catalyst in the form of a semiconductor. However, in the Glyoxal pathway, CO is produced alongside with CH_4 in ratio 1:1, exactly as observed in our study. According to our results, this mechanism is therefore very likely.

Our GC–MS analysis shows that together with CO and CH_4, several trace gases can be also detected in the resulting gas phase mixture. Methoxyacetaldehyde, acetaldehyde, acetic acid and acetone are products of oxidation processes on the photocatalyst surface and connection with the Glyoxal cycle mechanism can be tentatively followed as schematically depicted in Fig. 4, Panel B, route D.

Formation of chlorocarbons tetrachloromethane, trichloromethane and dichloromethane can be explained in two possible ways. The simplest explanation involves chlorination of CH_3 radical at the very end of the Glyoxal cycle [43] preceding formation of methane. This competitive process schematically summarized in Fig. 4, Panel B, route B, however, does not explain why monochloromethane was not detected among the products. Instead, high concentration of tetrachloromethane suggests that a parallel mechanism takes place alongside with methane formation. It can be tentatively expected that formation of formaldehyde in the Glyoxal cycle [43] can be alternated by formation of phosgene in the "cycle" involving chlorine. Such a mechanism results in at least dichloromethane. These assumptions motivate us for further explorations of this system using quantum chemical calculations as continuation of this purely experimental study.

4. Conclusion

Development of a sensitive analytical method for the determination of biogas and biogas-like mixtures composition is highly important to the field of environmental chemistry and artificial photosynthesis studies.

We show an application of combined techniques of FTIR, GC–MS and SIFT-MS analysis for determination of major constituents and traces in biogas and methane fuel produced by artificial photosynthesis.

The analysis of biogas shows several stages of the biogas production process and decreasing level of trace gases in older parts of landfill. Landfill biogas is also very rich in various trace gases involving corrosive hydrogen sulphide. All the samples of biogas contained methane and carbon dioxide in ratio 1:1. FTIR analysis shows that infrared spectrum is rich in various strong combination bands of methane and carbon dioxide. We assume that this analyte is perfectly suitable for analysis using gas sensors equipped with wafer-fused vertical-cavity surface-emitting lasers in combination with cheap novel InGaAs photodiodes that can operate at room temperature. This method was experimentally demonstrated for HF detection [40].

Methane fuel produced in artificial photosynthesis differs from composition of biogas. Carbon dioxide is not a product of this process, but it is consumed during synthesis of methane and carbon monoxide produced in ration 1:1. Similarly with biogas, acetone, acetaldehyde and acetic acid can be identified among the trace products. Our results show that mechanism of artificial photosynthesis can be well explained by Glyoxal cycle [43] over anatase A200 and for the first time observed in our study also over montmorillonite and graphene-anatase composite. Formation of chlorinated methane can be explained by parallel mechanism probably involving phosgene or chlorination of CH_3 radical in the Glyoxal cycle.

Methane biogas or fuels synthesized in artificial photosynthesis over acidic photocatalysts does not represent neat mixtures. Instead, inert (CO_2 in biogas) and corrosive gases such as H_2S in biogas, CCl_4, CCl_3H and CCl_2H_2 in artificial photosynthesis, are produced. Our study shows that a combination of FTIR, GC–MS and SIFT-MS techniques can represent suitable approach for further investigation of methane gas fuels synthesized in biogas or artificial photosynthesis systems in order to find the best photocatalyst and mixtures producing clean traces-free fuel suitable for fine applications such as utilization for energy production in gas engines, etc.

Contribution statement

MF and SC designed the research and performed FTIR analysis. KD and PŠ conducted SIFT-MS and GC–MS analysis. AK conducted photoreduction experiments. LK and MZ synthesized anatase samples. MF, SC, AK together with KD, PŠ, LK and MZ wrote the paper.

Acknowledgement

We thank the Czech Science Foundation, project 13-07724S, for supporting our research.

References

[1] J.P. Smol, Nature 483 (2012) S12–S15.
[2] National Oceanic and Atmospheric Administration, https://www.esrl.noaa.gov/gmd/ccgg/trends/, 2017.
[3] M. Aresta, A. Dibenedetto, Dalt. Trans. (2007) 2975–2992.
[4] I.E.A. in W. Energy, World Energy Outlook, 2011.
[5] P. Weiland, Appl. Microbiol.Biotechnol. 85 (2010) 849–860.
[6] S. Rasi, A. Veijanen, J. Rintala, Energy 32 (2007) 1375–1380.
[7] S.N. Habisreutinger, L. Schmidt-Mende, J.K. Stolarczyk, Angew. Chemie-Internation Ed. 52 (2013) 7372–7408.
[8] T. Inoue, A. Fujishima, S. Konishi, K. Honda, Nature 277 (1979) 637–638.
[9] O. Ishitani, C. Inoue, Y. Suzuki, T. Ibusuki, J. Photochem. Photobiol. A-Chem. 72 (1993) 269–271.
[10] M. Anpo, H. Yamashita, Y. Ichihashi, S. Ehara, J. Electroanal. Chem. 396 (1995) 21–26.
[11] G.R. Dey, A.D. Belapurkar, K. Kishore, J. Photochem. Photobiol. A-Chem. 163 (2004) 503–508.
[12] O.K. Varghese, M. Paulose, T.J. LaTempa, C.A. Grimes, NANO Lett. 9 (2009) 731–737.
[13] S.-I. In, D.D. Vaughn II, R.E. Schaak, Angew. Chemie-Int. Ed. 51 (2012) 3915–3918.
[14] L.-L. Tan, W.-J. Ong, S.-P. Chai, A.R. Mohamed, Nanoscale Res. Lett. 8 (2013).
[15] A.J. Morris, G.J. Meyer, E. Fujita, Acc. Chem. Res. 42 (2009) 1983–1994.
[16] J. Schneider, H. Jia, J.T. Muckerman, E. Fujita, Chem. Soc. Rev. 41 (2012) 2036–2051.
[17] D. Uner, M.M. Oymak, B. Ipek, Int. J. Glob. Warm. 3 (2011) 142–162.
[18] Y. Izumi, Coord. Chem. Rev. 257 (2013) 171–186.
[19] A. Zervos et al., Renewables 2016 Global Status Report, REN 21, Paris, 2016.
[20] G. Centi, S. Perathoner, ChemSusChem 3 (2010) 195–208.
[21] M. Ferus, Private communication with Analytical chemists in Troja Water Treatment Station, 2015.
[22] S. Civis, M. Ferus, P. Kubat, M. Zukalova, L. Kavan, J. Phys. Chem. C 115 (2011) 11156–11162.
[23] M. Ferus, L. Kavan, M. Zukalová, A. Zukal, M. Klementová, S. Civiš, J. Phys. Chem. C 118 (2014) 26845–26850.
[24] S. Civiš, M. Ferus, M. Zukalová, A. Zukal, L. Kavan, K.D. Jordan, D.C. Sorescu, J. Phys. Chem. C 119 (2015) 3605–3612.
[25] S. Civis, M. Ferus, M. Zukalova, L. Kavan, Z. Zelinger, Opt. Mater. (Amst). 36 (2013) 159–162.
[26] S. Civis, M. Bousa, A. Zukal, A. Knizek, P. Kubelik, P. Rojik, J. Novakova, M. Ferus, J. Phys. Chem. C 120 (2016) 508–516.
[27] L. Kavan, M. Zukalova, M. Ferus, J. Kuerti, J. Koltai, S. Civis, Phys. Chem. Chem. Phys. 13 (2011) 11583–11586.

[28] S. Civiš, M. Ferus, A. Knížek, P. Kubelík, L. Kavan, M. Zukalová, Opt. Mater. (Amst). 56 (2016).
[29] F.J. Harris, Proc. IEEE 66 (1978) 51–83.
[30] D.-76275 E. Bruker Optic GmbH, Rudolf-Plank-Straße 27, 2006, www.brukeroptics.com.
[31] D. Smith, P. Spanel, M.A.S.S. Spectrom, Rev. 24 (2005) 661–700.
[32] P. Spanel, D. Smith, Int. J. Mass Spectrom. 167 (1997) 375–388.
[33] P. Spanel, Y.F. Ji, D. Smith, Int. J. Mass Spectrom. 165 (1997) 25–37.
[34] P. Spanel, K. Dryahina, D. Smith, Int. J. Mass Spectrom. 249 (2006) 230–239.
[35] L.S. Rothman, I.E. Gordon, Y. Babikov, A. Barbe, D.C. Benner, P.F. Bernath, M. Birk, L. Bizzocchi, V. Boudon, L.R. Brown, A. Campargue, K. Chance, E.A. Cohen, L.H. Coudert, V.M. Devi, B.J. Drouin, A. Fayt, J.-M. Flaud, R.R. Gamache, J.J. Harrison, J.-M. Hartmann, C. Hill, J.T. Hodges, D. Jacquemart, A. Jolly, J. Lamouroux, R.J. Le Roy, G. Li, D.A. Long, O.M. Lyulin, C.J. Mackie, S.T. Massie, S. Mikhailenko, H.S.P. Mueller, O.V. Naumenko, A.V. Nikitin, J. Orphal, V. Perevalov, A. Perrin, E.R. Polovtseva, C. Richard, M.A.H. Smith, E. Starikova, K. Sung, S. Tashkun, J. Tennyson, G.C. Toon, V.G. Tyuterev, G. Wagner, J. Quant. Spectrosc. Radiat. Transf. 130 (2013) 4–50.
[36] S.A. Sandford, F. Salama, L.J. Allamandola, L.M. Trafton, D.F. Lester, T.F. Ramseyer, Icarus 91 (1991) 125–144.
[37] C.E. Miller, L.R. Brown, J. Mol. Spectrosc. 228 (2004) 329–354.
[38] J.C. Hilico, J. Degni, J.P. Champion, G. Guelachvili, J. Mol. Spectrosc. 81 (1980) 277–302.
[39] A. Predoi-Cross, L.R. Brown, V.M. Devi, M. Brawley-Tremblay, D.C. Benner, J. Mol. Spectrosc. 232 (2005) 231–246.
[40] S. Civis, Z. Zelinger, V. Nevrly, A. Dorogan, M. Ferus, V. Iakovlev, A. Sirbu, A. Mereuta, A. Caliman, G. Suruceanu, E. Kapon, J. Quant. Spectrosc. Radiat. Transf. 147 (2014) 53–59.
[41] V.G. Anicich, An index of the literature for bimolecular gas phase cation-molecule reaction kinetics, Technical Report No. JPL-Publ-03-19, https://ntrs.nasa.gov/search.jsp?R=20060029368, Pasadena, California, 2003.
[42] I. Angelidaki, L. Ellegaard, B.K. Ahring, Biotechnol. Bioeng. 63 (1999) 363–372.
[43] I.A. Shkrob, T.W. Marin, H. He, P. Zapol, J. Phys. Chem. C 116 (2012) 9450–9460.
[44] R.K. Thauer, Microbiol.-UK 144 (1998) 2377–2406.
[45] P. Michal, Bioplyn – energie ze zemědělství, Informační Přehledy ÚZPI, 2005.
[46] A. Knížek, M. Zukalová, L. Kavan, A. Zukal, P. Kubelík, P. Rojík, P. Skřehot, M. Ferus, S. Civiš, Appl. Clay Sci. 137 (2016) 6–10.
[47] S. Civis, M. Ferus, J.E. Sponer, J. Sponer, L. Kavan, M. Zukalova, S. Civiš, Chem. Commun. 50 (2014) 7712–7715.
[48] S. Civis, M. Ferus, M. Zukalova, P. Kubat, L. Kavan, J. Phys. Chem. C 116 (2012) 11200–11205.
[49] I.A. Shkrob, N.M. Dimitrijevic, T.W. Marin, H. He, P. Zapol, J. Phys. Chem. C 116 (2012) 9461–9471.